Biosensors and Bioelectronics 184 (2021) 113238

Contents lists available at ScienceDirect

Biosensors and Bioelectronics

journal homepage: http://www.elsevier.com/locate/bios

Nanomaterial-enhanced 3D-printed sensor platform for simultaneous detection of atrazine and acetochlor

Xiaofan Ruan [a], Yijia Wang [a], Eunice Y. Kwon [b], Limin Wang [a], Nan Cheng [a], Xiangheng Niu [a], Shichao Ding [a], Bernard J. Van Wie [b], Yuehe Lin [a], Dan Du [a,*]

[a] School of Mechanical and Materials Engineering, Washington State University, Pullman, WA, 99164-2920, United States
[b] Voiland School of Chemical Engineering and Bioengineering, Washington State University, Pullman, WA, 99164-6515, United States

ARTICLE INFO

Keywords:
Lateral flow immunoassay
palladium@platium nanoparticle
Electrochemical analysis
3D-printing
Multiplex biosensor

ABSTRACT

The widespread use of herbicides in agriculture and gardening causes environmental and safety issues such as water pollution. Thus, efficient and convenient analysis of the levels of herbicide residues is of significant importance. Here, we employed 3D-printing to design a multiplex immunosensor for simultaneous detection of two widely used herbicides, atrazine and acetochlor. Multiplexing was achieved through customization of a lateral flow immunoassay, and then integrated with an electrochemical analyzer for ultrasensitive detection. Quantification of herbicide residues was realized through the detection of a novel nanomaterial label, the mesoporous core-shell palladium@platium nanoparticle (Pd@Pt NP), for its outstanding peroxidase-like property. During the electrochemical analysis, the catalytic activity of Pd@Pt NPs on the redox reaction between thionin acetate and hydrogen peroxide provided an electrochemically driven signal that accurately indicated the level of herbicide residues. Using this Nanomaterial-enhanced multiplex electrochemical immunosensing (NEMEIS) system, simultaneous detection of atrazine and acetochlor was realized with a limit of detection of 0.24 ppb and 3.2 ppb, respectively. To further evaluate the feasibility, the optimized NEMEIS was employed for detection in atrazine and acetochlor residue-containing spiked samples, and an overall recovery with 90.8% – 117% range was obtained. The NEMEIS constructed with the aid of 3D-printing provides a rapid, precise, economical, and portable detection device for herbicides, and its success suggests potential broad applications in chemical analysis, biosensors and point-of-care monitoring.

1. Introduction

Atrazine and acetochlor are among the most widely used herbicides worldwide (Liu et al., 2017; Sousa et al., 2018). Although atrazine, which belongs to triazine group, has been banned in a few countries due to safety issues, its resulting residues in the environment, e.g., groundwater, are still among the highest levels compared to residues of other herbicides (Hvězdová et al., 2018). Acetochlor which belongs to the group of chloroacetanilide is now strictly restricted for use because of its potential harm as a human carcinogen and its influence on fish and other aquatic animals (Arregui et al., 2010; Xie et al., 2019). Therefore, precise and efficient detection of these herbicide residues is a serious environmental concern.

Current techniques to detect atrazine, acetochlor, and other herbicides with relatively small molecular sizes rely on expensive analytical facilities such as gas chromatography (GC) and high-performance liquid chromatography (HPLC) in laboratorial environments. Although they allow very sensitive and selective detection, these facilities have limited use for point-of-care and rapid detection at low cost. Thus, efforts have been made to develop alternative approaches that embrace onsite detection formats while maintaining quality detection performance standards (Mehrotra, 2016). Typical examples of these approaches are biosensors based on signal enhancement through the use of natural bio-recognition (Liu et al., 2016). For instance, some take advantage of complementary nucleic acid probes (Du and Dong, 2017; Jayanthi et al., 2017) and immunoassay methods, through which high selectivity can be achieved (Shu and Tang, 2017; Skládal, 1997; Zou et al., 2010). Among these approaches is the paper-based lateral flow immunoassay (LFIA) as this technology proves to be economical, portable and easy to handle even for untrained persons (Sajid et al., 2015; Zhang and Liu, 2016). The LFIA technology has been widely used in point-of-care (POC) devices to qualitatively detect the existence of analytes, including

* Corresponding author.
E-mail address: annie.du@wsu.edu (D. Du).

https://doi.org/10.1016/j.bios.2021.113238
Received 24 November 2020; Received in revised form 15 March 2021; Accepted 6 April 2021
Available online 10 April 2021

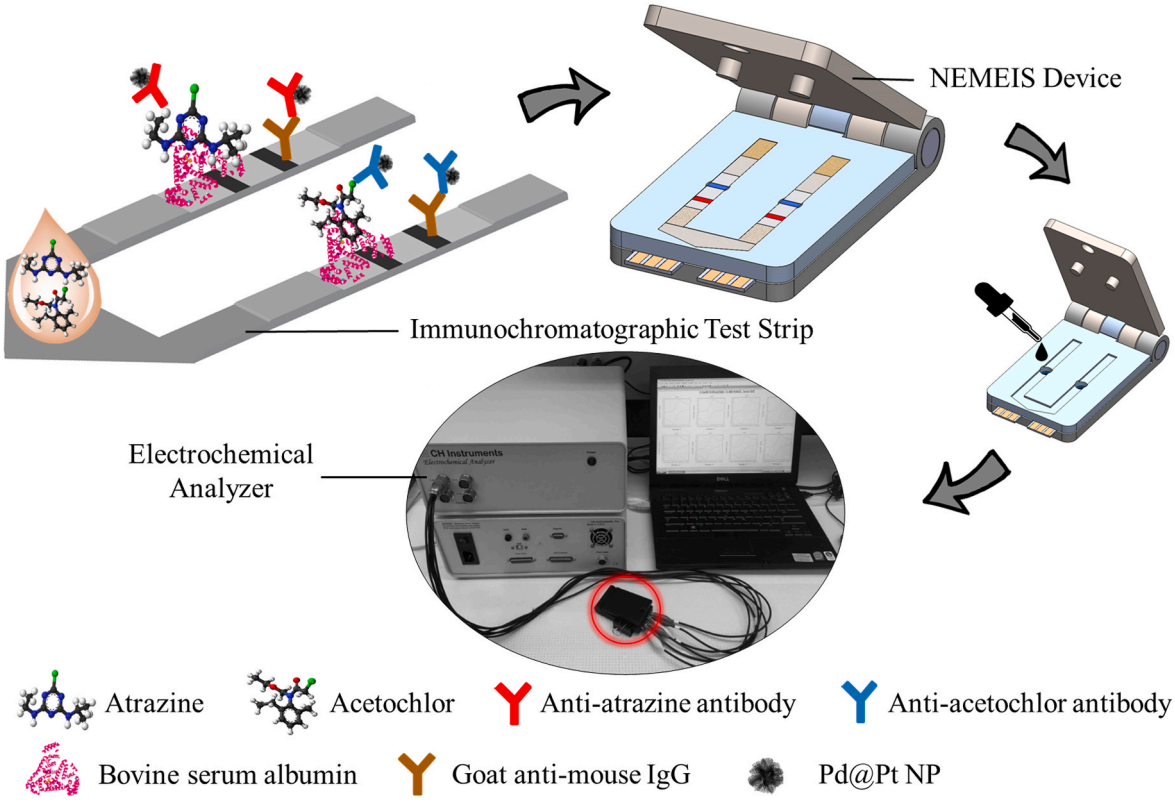

Scheme 1. Nanomaterial-enhanced multiplexed electrochemical immunosensing system (NEMEIS).

organophosphorus compounds, pathogens, and glucose (Tang et al., 2000; Zhou et al., 2018). Certain LFIA approaches, like those used for detecting HIV, have been commercialized validating the reliability of the approach. However, LFIA applications remain limited due to the inherent defect of lacking the ability for ultrasensitive and quantitative readouts (Mudanyali et al., 2012; Pai et al., 2007). Thus, further improvement in LFIA technology is necessary.

To improve the sensitivity of LFIA-based detection, various biosensing platforms such as electrochemical, optical, and mass-based detection platforms, have been studied to be integrated with LFIA (Kumar et al., 2018; Mahato et al., 2017). In particular, electrochemical analysis has been widely employed to detect analytes quantitatively with outstanding sensitivity (Cesarino et al., 2012; Du et al, 2010, 2011; Sahin and Kaya, 2019; Taleat et al., 2014). An electrochemical analyzer uses conductive electrodes to evaluate the electrical information in solution to determine the total amount of analyte. The sensitivity of detection largely depends on the electrochemical scanning methods, the chemical mechanism of reactions, and detecting platforms (Madurai veeran et al., 2018). One design strategy is to directly fabricate electrodes using manufacturing techniques such as inkjet-printing on a paper-based platform; another is to re-disperse the part of electrochemically active indicators in solution after the LFIA process, thereby allowing the electrochemical assessment (Mettakoonpitak et al., 2016). However, both strategies require additional manufacturing or transfer steps that can result in inferior reproducibility and reliability, limiting ultrasensitive diagnosis and assessment.

Overcoming LFIA-related challenges requires a properly designed platform to efficiently integrate LFIA strips with electrochemical analyzers. With this goal in mind, we employed emerging 3D-printing technology with flexible, customized, economical and rapid prototyping capability. 3D-printing has attracted significant attention over the past decades in materials manufacturing and analytical chemistry (Gross et al., 2017; Ho et al., 2018; Mao et al., 2017; Rim et al., 2016); it has enabled fabrication for many biosensor applications from the nanoscale to macroscale (Ambrosi and Pumera, 2016; An et al., 2015; Sharafeldin et al., 2018; Zhang et al., 2016), and significant progress has been reported for portable POC biosensing and medical devices (Ruan et al., 2020; Sharafeldin et al., 2018). A typical trend is to use 3D-printed smartphone-based colorimetric devices that use a camera and corresponding software to analyze colorimetric information for enzyme-linked immunosorbent assay (ELISA). This type of approach exhibits improved portability and economy, and similar sensitivity to that of conventional analytical techniques (Cevenini et al., 2016; Choi et al., 2016; Dou et al., 2016; Ji et al., 2017; Roda et al., 2014; Wang et al., 2017).

However, natural enzymes have significant applications in industrial, medical, and biological arenas due to high substrate selectivity and catalytical efficiency, while intrinsic drawbacks including low stability and activity under harsh conditions, high cost of preparation, purification and storage, and low reusability, have promoted exploration on the use of artificial enzymic mimicking materials (Wang et al., 2018). Progress has been achieved in the use of various nanomaterials including precious metal-based materials such as Pt, Pd, and Au nanoparticles and their bi/trimetallic composites, non-precious metal-based nanomaterials such as Fe_3O_4, CeO_2, MnO_2, MOFs, and ZIFs, and carbon/graphene-based nanomaterials (Huang et al., 2019; Niu et al., 2020). Pt-Pd bimetallic nanoparticles are an attractive class featuring superior peroxidase mimicking properties due to bimetallic synergy and a mesoporous core-shell structure, which provides large surface area with abundant active sites, as well as excellent chemical stability and good dispersibility in a water matrix (Hossain and Park, 2014; Jiang et al., 2016; Yuan et al., 2014). Moreover these materials have been shown by our group to be stable over broad 1–11 pH and 4–90 °C temperature range (Jiang et al., 2016).

In this paper we report on the use of 3D printing techniques applied to fabrication of a high-performance multiplex biosensor to detect herbicide residues. Our biosensor as depicted in Scheme 1 combines the advantages of the LFIA and electrochemical analysis, i.e.: i) the

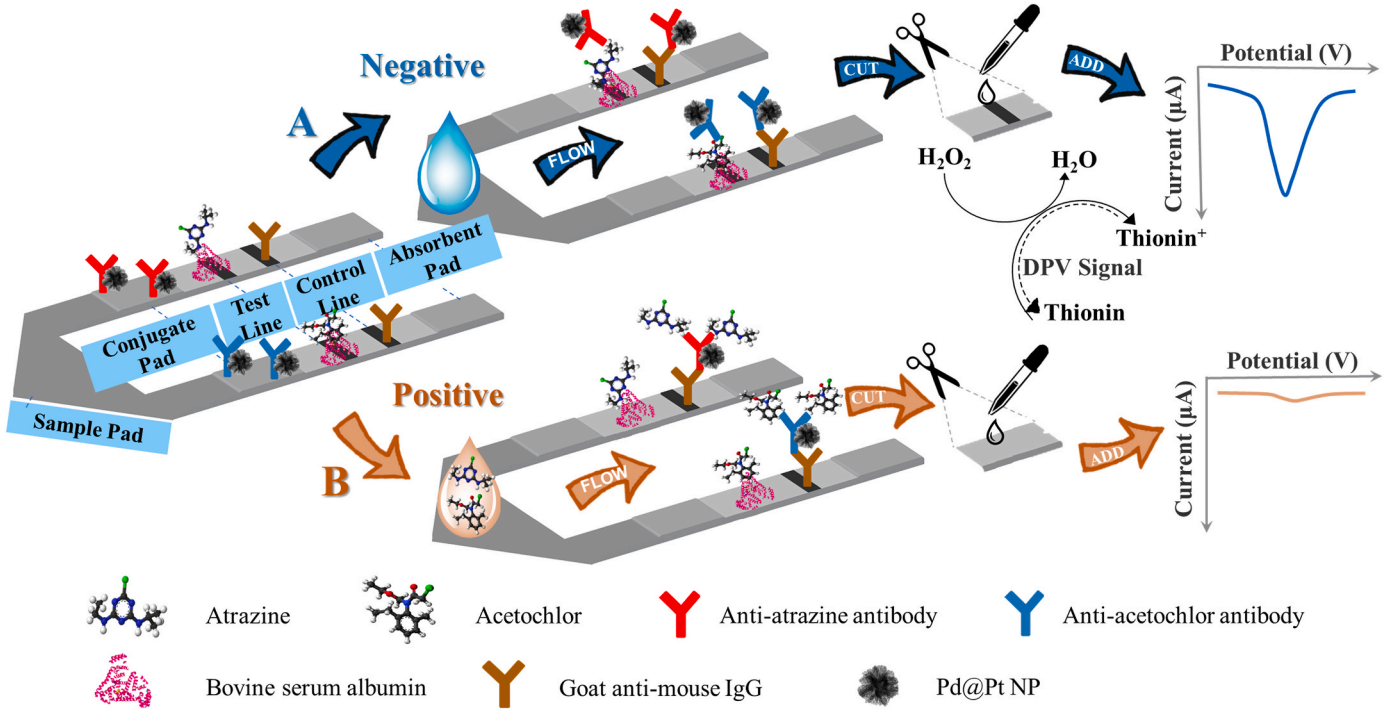

Scheme 2. Principle of NEMEIS: (from left to right) the fabrication of bifurcated immunochromatographic strips; the multiplex competitive lateral flow immunoassay (LFIA) and the electrochemical quantification of targets.

capability of portable economical onsite rapid detection; and ii) ultrasensitive quantification of herbicide residues. Mesoporous core-shell palladium@platinum nanoparticles (Pd@Pt NPs) which have superior catalytic activity are used as an antibody label to enhance the biorecognition process and as an electrochemically active indicator for the quantitative assessment of herbicide residues (Kurbanoglu et al., 2017; Zhao et al., 2018). The 3D-printed device provides a stable and reliable system that can combine the LFIA technology with an electrochemical analyzer to reduce detection error generated from colorimetric based readouts. Results for use of this nanomaterial-enhanced multiplex electrochemical immunosensing (NEMEIS) system when applied to detect atrazine and acetochlor will be presented. We will discuss the advantages of the NEMEIS as a promising versatile technique and an alternative to laboratory-based facilities for extending applications to other ultrasensitive analyses in a portable format for onsite environmental and bedside health monitoring and disease diagnosis.

2. Experimental section

2.1. Materials

Atrazine ($C_8H_{14}ClN_5$), acetochlor ($C_{14}H_{20}ClNO_2$), Tween-20, Pluronic F-127, 3,3′,5,5′-tetramethylbenzidine (TMB) liquid substrate system (peroxidase substrate), bovine serum albumin (BSA), thionin acetate ($C_{12}H_9N_3S$-$C_2H_4O_2$), sodium tetrachloropalladate(II) (Na_2PdCl_4), L-ascorbic acid, sucrose, and potassium carbonate (K_2CO_3) were purchased from Sigma-Aldrich (St. Louis, MO, USA). Atrazine antigen (atrazine-BSA) and atrazine monoclonal antibody were purchased from MyBioSource Inc. (San Diego, CA, USA). Acetochlor antigen (acetochlor-BSA) and acetochlor monoclonal antibody were purchased from Creative Diagnostics (Shirley, NY, USA). Goat-anti-mouse IgG antibody, hydrogen peroxide, and potassium tetrachloroplatinate(II) ($K_2[PtCl_4]$) were purchased from Thermal Fisher Scientific Inc. (Waltham, MA, USA). Phosphate buffered saline (0.01 M, 1 × PBS, pH 7.4) was purchased from RICCA Chemical Company (Arlington, TX, USA). Hydrochloric acid, LFIA membrane cards, glass fiber conjugate pad sheets and fiber absorbent pads were purchased from Millipore Sigma (Burlington, MA, USA). Screen-printed electrodes (ET077-40) were purchased from eDAQ Inc. (Colorado Springs, CO, USA).

2.2. Designing and printing accessory devices utilizing 3D-printing

A fused deposition modeling (FDM) based 3D printer, Einstart-S (Shining 3D technology Inc. San Francisco, CA, USA), was employed to fabricate the accessory devices using a polylactic acid filament. The FDM 3D printing technique was employed because it is widely accepted as the simplest way to achieve 3D printing with high efficiency and reliability at relatively low cost compared to other techniques like stereolithography and inkjet printing (Ruan et al., 2020). The CAD file of the device was produced through SolidWorks (Dassault Systèmes SolidWorks Corporation, Waltham, MA, USA). Detailed design drawings are shown in Fig. S1 showing the device comprised of a strip cutter, a strip holder, and an electrode holder with two built-in reaction cells, with an overall size of 80 mm × 50 mm × 15 mm.

2.3. Preparation and characterization of Pd@Pt NPs

Pd@Pt NPs were fabricated using previously reported approaches with modifications (Cheng et al., 2017; Zhu et al., 2015). First, a solution mixture made by combining 3.6 mL of 20 mM potassium tetrachloroplatinate(II), 0.4 mL of 20 mM sodium tetrachloropalladate(II), 4 mL of 100 mM L-ascorbic acid, 88 μL of 6 mol/L hydrochloric acid, and 20 mg of Pluronic F-127 was heated to 35°C and exposed to ultrasonic treatment for 4 h in an ultrasonic cleaner (Ultrasonics Direct, Pontiac MI, USA). This results in the synthesis of Pd@Pt NPs product which was then centrifuged at 12,000 rpm for 8 min, followed by washing with acetone for 3 times and then with water for 3 times. Finally, the Pd@Pt NPs were dispersed in 5 mL of water. Transmission electron microscope (TEM) images were captured with a Technai G2 20 Twin instrument with a 200 KV LaB6 electron source. Scanning electron microscopy (SEM) images were obtained with an FEI Quanta 200F instrument.

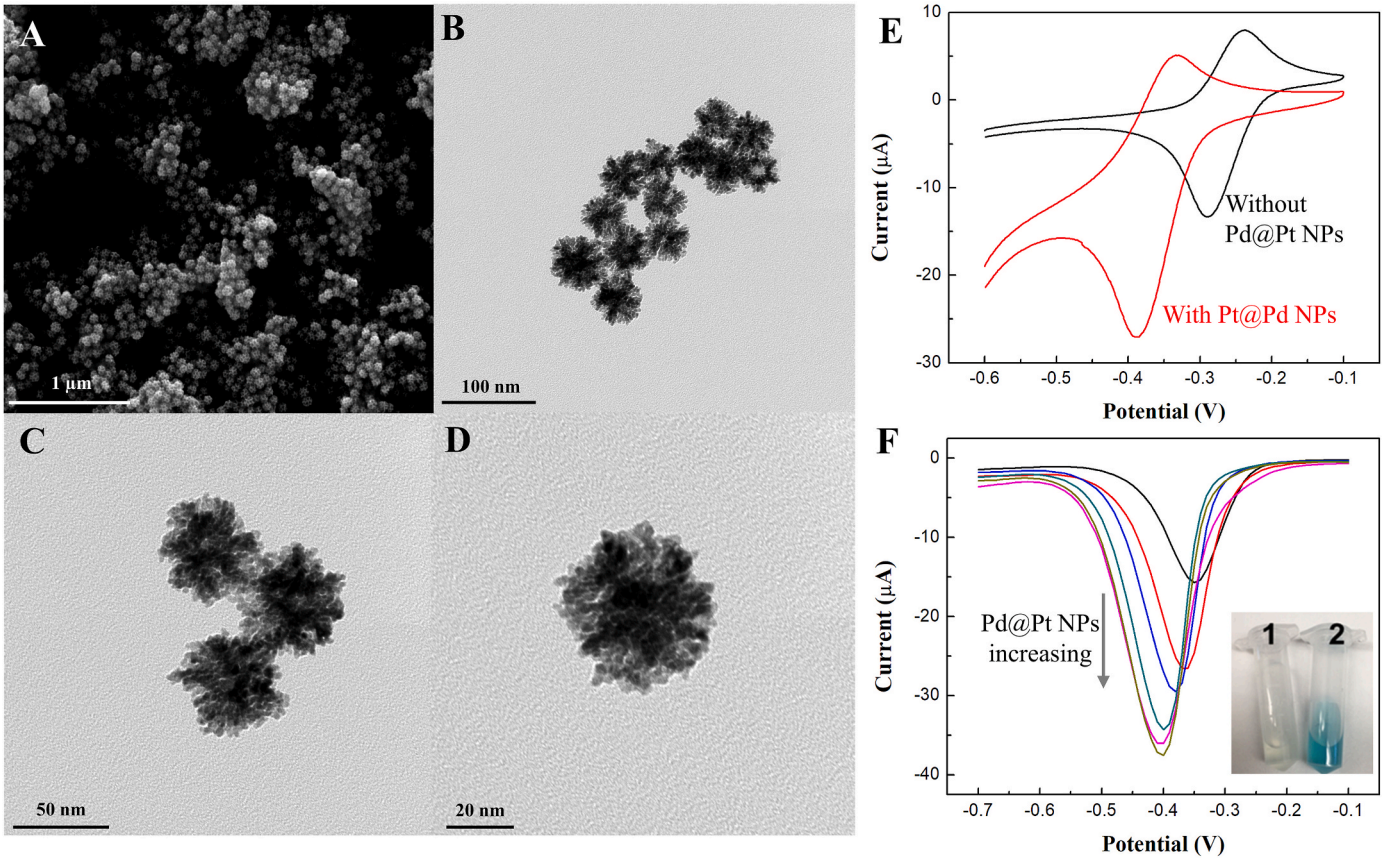

Fig. 1. SEM image (A); TEM images (B–D) of Pd@Pt NPs. And peroxidase-like activity of Pd@Pt NPs: the electrochemical results from CV curves (E) for the redox of 1 mM thionin acetate and 50 mM hydrogen peroxide with and without the existence of 10 μL of 1 mg/mL Pd@Pt NPs. And the DPV curves (F) generated from the same substrate of (E) after incubation with 10 μL of 10 ng/mL, 0.1 μg/mL, 1 μg/mL, 10 μg/mL, 0.1 mg/mL, and 1 mg/mL of Pd@Pt NPs, respectively. The colorimetric assay depicted in the inset of (F) provides visual validation of the catalytic property of Pd@Pt NPs for the oxidation of TMB as the solution becomes blue when TMB is oxidized: 1) Control; 2) Pd@Pt NPs added. (For interpretation of the references to color in this figure legend, the reader is referred to the Web version of this article.)

2.4. Preparation of antibody-Pd@Pt NP conjugates

The antibody-nanoparticle conjugates were fabricated through electrostatic adsorption using a previously reported approach (Zhu et al., 2015). The suspension liquid of the prepared Pd@Pt NPs is divided into two parts, followed by adjusting pH to A) 8.20–8.25 and B) 8.10–8.15 by adding potassium carbonate (0.02 mol/L). Then, 10 μL of 0.5 mg/mL atrazine monoclonal antibody and 10 μL of 0.5 mg/mL acetochlor monoclonal antibody were added into A and B, respectively, followed by continuous mixing at room temperature on a 3D rotator (Lab-line BioSurplus, San Diego, CA, USA) for 1 h. Then 10.0% BSA was added to each of A and B and incubated at room temperature for 30 min in an Analog Incubator (Quincy Lab, Chicago, IL, USA). Finally, the conjugates were centrifuged at 12,000 rpm for 8 min, washed 5 times with 0.01 M (pH 7.4) phosphate buffered saline containing 1.0% BSA, and re-suspended in 200 μL of 0.01 M (pH 7.4) phosphate buffered saline containing 2.0% BSA and 3.0% sucrose. Herein, the resulting conjugates are referred to as Ab-Pd@Pt NPs. Successful conjugation was validated using zeta potential analysis on a Zetasizer Nano ZS (Malvern Instruments, Inc., Westborough, MA) with results presented in the supporting information (Figure S3). The zeta potential of Pd@Pt NPs reduces from -34.7 mV to -16.8 mV and -15.6 mV after conjugation with anti-atrazine and anti-acetochlor antibody, respectively. The Ab-Pd@Pt NPs form by passive absorption through electrostatic interactions at a pH slightly higher than the isoelectric point of each antibody; thus, the negatively charged NPs will tightly bind to positively charged groups associated with an antibody macromolecule.

2.5. Preparation of bifurcated immunochromatographic test strips

Each LFIA strip was composed of a sample pad, a conjugate pad, a nitrocellulose membrane, and an absorbent pad on an adhesive polyvinyl chloride backing card. The bifurcated LFIA strips illustrated in Scheme 2 consist of two 12 mm × 4 mm absorbent pads, two 25 mm × 4 mm nitrocellulose membranes, two 10 mm × 4 mm conjugate pads and a shared 25 mm × 9 mm triangle sample pad. Strips were cut and shaped with the use of a CM4000 guillotine cutter (BioDot, Irvine, CA, USA). Each conjugate pad underwent preparation by infiltration of BSA and sucrose solution followed by drying overnight before use. The infiltration treatment details were determined as part of this study; it will be discussed in the LFIA optimization section. The control lines on both channels were created by dispensing 1 mg/mL goat-anti-mouse IgG antibody (using an XYZ3050 dispenser platform (BioDot, Irvine, CA, USA). The test lines were created by dispensing 1 mg/mL antigen, either atrazine-BSA for one side of the strip or acetochlor-BSA for the other side. The dispensed strips were then dried overnight at room temperature. Finally, 2.5 μL of each of the respective types of the synthesized Ab-Pd@Pt NPs were coated onto the conjugate pad to complete the preparation of the LFIA strips before use.

2.6. Competitive lateral flow immunoassay procedure

To test the system, the bifurcated immunochromatographic test strip is placed in the strip holder as presented in Schemes 1 and 2 in the NEMEIS device, and 200 μL of herbicide solution is applied onto the

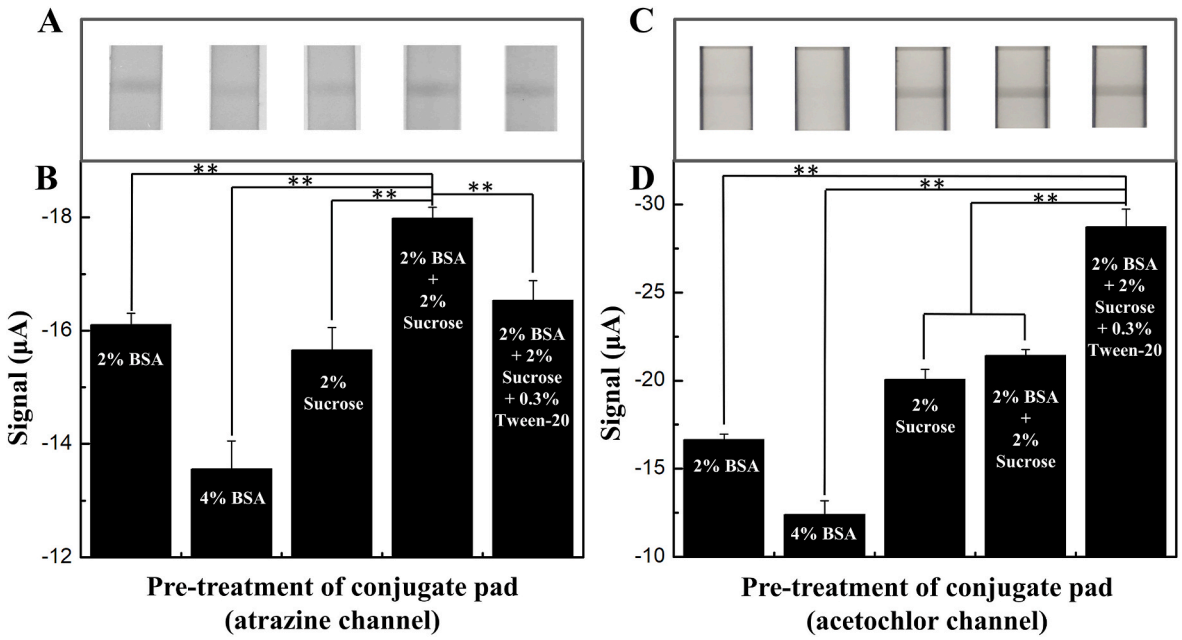

Fig. 2. Optimization of the pre-treatment of conjugate pads with various buffer solutions. Visualization of test line results for the LFIA (A) and results of electrochemical analysis using the NEMEIS (B) for atrazine channels, and respective trends for acetochlor channels (C) & (D). (*p-value < 0.05 means the difference is significant; **p-value < 0.005 means the difference is very significant.)

sample pad. The sample solution migrates toward the absorbent pads of the bifurcated channels driven by the capillary forces. A time frame of 10 min is allowed for the LFIA to complete, and a dark color is observed on the test lines and control lines, indicating the successful capture of Ab-Pd@Pt NPs. While the visual observation of the dark NPs associated test or control lines may be used for qualitative recognition of herbicide at this point, the quantitative amount of retained Ab-Pd@Pt NPs on the test lines is assessed through the electrochemical assay described in the next section.

2.7. Electrochemical assay procedure to determine the concentrations of each herbicide

The amount of Ab-Pd@Pt NPs on the test lines can be determined through their overall catalytic activity on the redox reaction between thionin acetate and hydrogen peroxide. First, test line sections of the LFIA strips are snipped by the cutter protruding from the lever arm and dropped into the O-ring sealed reaction cells located immediately beneath them (Scheme 1). Before covering and sealing, the cells containing screen-printed electrodes at the bottom receive an 80 μL liquid drop comprised of 1 mM thionin acetate and 50 mM hydrogen peroxide. After the incubation for 2 min, the corresponding redox reaction is monitored by differential pulse voltammetry (DPV) scanning from -0.1 to -0.7 V, with a scanning amplitude of 0.02 V and pulse width of 0.05 s, using a CHI1030A multi-potentiostat (CH Instruments, Austin, TX).

3. Results and discussion

3.1. Principle of multiplex competitive lateral flow immunoassay

As anticipated and illustrated in Scheme 2, when a 200 μL sample containing abundant atrazine and acetochlor on the order of 10^3 ppb herbicide was dropped on the sample pad, liquid flowed toward the absorbent pad through the capillary forces. The herbicides, atrazine and acetochlor, were successfully captured by corresponding Ab-Pd@Pt NPs loaded on the conjugate pads as evidenced that the Ab-Pd@Pt NPs were unable to be captured by the test lines where corresponding haptens were immobilized; however, they were captured by goat-anti-mouse antibody at the control lines as resulted in the black control line (Scheme 2B, Positive). Alternatively, when no herbicide is present in the sample solution, Ab-Pd@Pt NPs were captured by the immobilized BSA-herbicide at the test line; therefore, the black test lines appeared as shown in Scheme 2A (Negative). Given that only free Ab-Pd@Pt NPs are captured and retained on the test lines as a result of the competitive reaction, the amount of Ab-Pd@Pt NPs on the test lines is inversely dependent on the concentration of herbicide residues in the sample solution. The entire competitive LFIA process takes about 10 min. This will be verified quantitatively in Section 3.5.

3.2. Characterization of Pd@Pt NPs

The microstructure of the synthesized Pd@Pt NPs was characterized through SEM and TEM (Fig. 1A–D). The Pd@Pt NPs present mesoporous core-shell structures with an average particle size of ~50 nm. The catalytic activity of Pd@Pt NPs as reported in previous work reported from our labs (Fu et al., 2016; Zhao et al., 2018) was re-validated here through colorimetric and electrochemical assays: i) A colorimetric assay was conducted, with the results presented in Fig. 1F (Insets 1&2). 2.5 μL of Pd@Pt NPs at a concentration of 1 mg/mL was added into 200 μL of commercial TMB and hydrogen peroxidase mix substrate; blue color was produced through the oxidation of TMB. The peroxidase-like activity of Pd@Pt NPs induces the generation of hydroxyl radicals from hydrogen peroxidase, and these radicals then oxidize the TMB substrate and produce the diimine oxidation product having a blue color; ii) An electrochemical assay was conducted to validate the catalytic property of Pd@Pt NPs for the redox reaction of thionin acetate and hydrogen peroxidase. The cyclic voltammetry (CV) and differential pulse voltammetry (DPV) curves are presented in Fig. 1E&F, both of which show increased reduction peaks with the adding of Pd@Pt NPs, as the result of more thionine_{ox} generated under the catalysis of Pd@Pt NPs.

3.3. Principle of the nanomaterial-enhanced multiplex electrochemical immunosensing system

Ab-Pd@Pt NPs loaded test lines of the bifurcated LFIA strips were snipped and dropped into the electrochemical reaction cells above the

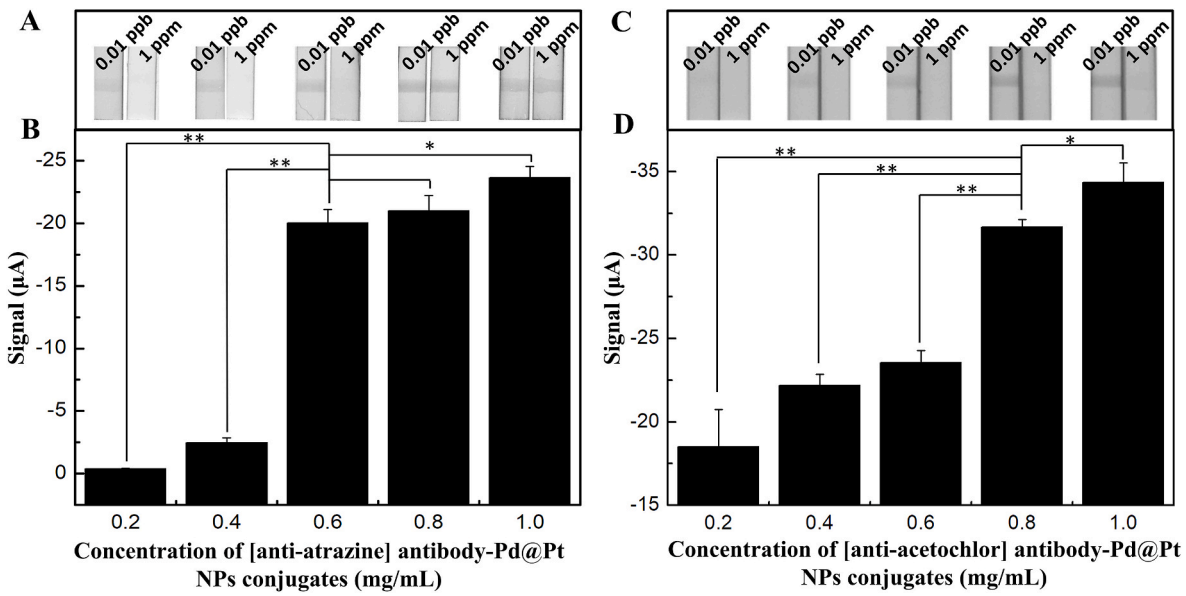

Fig. 3. Optimization of concentration of Ab-Pd@Pt NPs. Colorimetric results of the LFIA (A) and results of electrochemical analysis using the NEMEIS (B) for [anti-atrazine]-Ab-Pd@Pt NPs, and for [anti-acetochlor]-Ab-Pd@Pt NPs (C) (D). (*p-value < 0.05 means the difference is significant; **p-value < 0.005 means the difference is very significant.)

SPEs in the device. In the electrochemical reaction cell, the Pd@Pt NPs with high peroxidase-like catalytic activity served as the indicator of the total load of Ab-Pd@Pt NPs retained in the test lines (Choi et al., 2020; Du et al., 2011). As stated earlier the Pd@Pt NPs catalyze the oxidation of thionine in the existence of hydrogen peroxidase, raising the concentration of $thionine_{ox}$, which induces an electrochemical reduction peak expressed in CV and DPV curves. The peak current signal values of the DPV curves correspond to the strength of the catalytic effect and are negatively correlated with the concentrations of herbicides in the sample. Thus, with the completion of a competitive immunoassay followed by an electrochemical analysis, the concentrations of atrazine and acetochlor are deduced based on the load of Pd@Pt NPs on each test line of LFIA strips. The amounts are quantitatively evaluated from calibration curves based on the peak current signals from corresponding DPV curves as will be described below.

3.4. Optimization of the detection system

To achieve the best detection performance of the bifurcated immunochromatographic test strips, two crucial parameters were optimized: the pre-treatment steps for the conjugate pads; and the concentration of Ab-Pd@Pt NPs loaded onto the pads. Porous glass fiber pads, with an average cross-sectional diameter of 7.5 μm and a thickness of 0.41 mm were used as the reservoir for the labeled antibody complex with low nonspecific adsorption and good uniformity. The preparation procedures for the conjugate pads should be optimized to allow the optimal delivery of the complex to the capture line (test line) on the NC membrane. The conjugate pads were undergone the infiltration treatment with five solutions: 2% BSA; 4% BSA; 2% sucrose; 2% BSA + 2% sucrose; and 2% BSA + 2% sucrose + 0.3% Tween-20: i) As presented in Fig. 2, the optimal pre-treatment of the conjugate pads for the anti-atrazine antibody complex ([anti-atrazine] Ab-Pd@Pt NPs) was found, when using 0.01 ppb of atrazine and acetochlor test solutions, to be the 2% BSA + 2% sucrose solution. This is supported by the fact that test lines are darker (Fig. 2A) and more importantly DPV peaks are statistically largest for this solution, i.e. 8.7% higher than the next best 2% BSA + 2% sucrose + 0.3% Tween-20 solution indicating more abundant capture of the antibody complex (Fig. 2B). ii) The optimal pre-treatment of the conjugate pads for the anti-acetochlor antibody complex ([anti-acetochlor]-Ab-Pd@Pt NP) was found to be the 2% BSA + 2% sucrose + 0.3% Tween-20 solution. This is supported by the fact that again test lines are darker (Fig. 2C) and in this case, the DPV peaks are statistically larger by 34% in contrast to those for the next best 2% BSA + 2% sucrose indicating more abundant capture (Fig. 2D). More importantly, these results infer that the respective optimal pre-treatments result in lower nonspecific adsorption of the Ab-Pd@Pt NPs within the conjugate pad and better delivery of complexes to the herbicide-BSA test line area.

Of equal importance is the optimization of the concentration of Ab-Pd@Pt NPs loaded on the conjugate pads. An excessive concentration of Ab-Pd@Pt NPs can increase background noise, thereby limiting the sensitivity. Meanwhile too low of a concentration can result in signals so weak that increases in Ab-Pd@Pt binding are indiscernible over controls or that one cannot discern the differences between herbicide concentrations. Therefore, a series of concentrations of 0.2, 0.4, 0.6, 0.8 and 1.0 mg/mL of the Ab-Pd@Pt NPs (2.5 μL) were loaded onto the conjugate pads and optimums were determined for each herbicide. Relative test lines were evaluated for two concentrations, 0.01 ppb and 1 ppm, to assess both signal strength and background noise for each assay group. In Fig. 3B, the electrochemical results for samples containing 0.01 ppb atrazine and 0.01 ppb acetochlor showed a statistically significant increase in signal strength at a concentration of 0.6 mg/mL Ab-Pd@Pt NPs with a 716% increase than that of the 0.4 mg/mL concentration; however, there was no significant change in signal strength thereafter. Also, as indicated in Fig. 3A, the maximum contrast occurs here indicating the lowest background noise. It is important to view these results in contrast to the LFIA images for the 1 ppm atrazine. For the 0.6 mg/mL Ab-Pd@Pt NPs, signals of the test lines at the 1 ppm concentration are indiscernible visually; therefore, the assay can be used for accurate measurements between the 0.01 ppb to 1 ppm range. At 0.8 and 1 mg/mL Ab-Pd@Pt NPs levels, however, the differences between the 0.01 ppb and 1 ppm became less distinct; this indicated that an overabundance of Ab complex resulted in significant binding at the test line in spite of two orders of magnitude difference in concentration of herbicide that makes the assay unreliable over this range. Applying the same methodology to Fig. 3C&D to optimize the concentration of [anti-acetochlor] Ab-Pd@Pt NPs, a significant 35% increase appeared in signal strength between 0.6 and 0.8 mg/mL; however, there was an insignificant change thereafter for the 1 mg/mL concentration. While there was still a fairly sharp contrast between the 0.01 ppb and 1 ppm acetochlor concentrations at the 1 mg/mL Ab-Pd@Pt NPs concentration, there is no need to use the

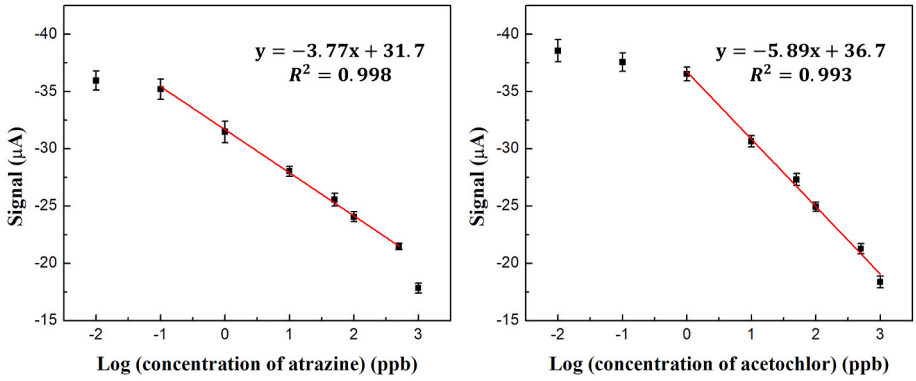

Fig. 4. The standard curves for the detection of atrazine (left) and acetochlor (right) using NEMEIS.

additional conjugate especially at the risk of losing sensitivity.

3.5. Assessing the performance for the detection of atrazine and acetochlor

The performance of the optimized NMEIS was assessed for detecting samples of various concentrations of atrazine and acetochlor. As presented in Fig. 4, there were linear relationships between the peak current signals and the concentrations of atrazine and acetochlor. A linear range of the detection for atrazine was obtained from 0.1 to 500 ppb with a relationship of I = -3.77 log (C_{Atr} [ppb]) + 31.7 where I is the peak current value, with R^2 = 0.998; and a linear detection range for acetochlor was obtained from 1 to 1000 ppb with a relationship of I = -5.89 log (C_{Ace} [ppb]) + 36.7 with R^2 = 0.993. In reality we want to use the system to report ppb values as a function of peak currents. Therefore the equations would need to be rewritten for atrazine to be $C_{Atr}[ppb] = \sqrt[3.77]{10^{31.7-I}}$ and for acetochlor to be $C_{Ace}[ppb] = \sqrt[5.89]{10^{36.7-I}}$. Based on a signal-to-noise ratio of three standard deviations, i.e., S/N = 3, the limits of detection (LODs) for atrazine and acetochlor are determined to be 0.24 and 3.2 ppb, respectively. The sensitivities of this method are better than the ~388 ppb for atrazine reported by Liu et al. using a molecular imprinting fluorescent assay, the 170 ppb for acetochlor reported by Tan et al. using the GC/MS technique, and in line with the most accurate values for atrazine of 0.1 ppb reported by Zhao et al. using an HPLC technique and that for acetochlor of 10 ppb reported by Yu et al. using GC/MS technologies (Liu et al., 2011; Tan et al., 2014; Yu et al., 2019; Yuan et al., 2018; Zamaleeva et al., 2011; Zhao et al., 2015). The proposed device and approach also present superior sensitivities and/or ranges of detection compared to other immunoassay approaches and lateral flow methods (Cheng et al., 2019; Deryabina et al., 2005; Kaur et al., 2007; Kwon et al., 2020).

To further demonstrate the performance of NEMEIS, spiked samples in natural water matrices were used for spike-recovery tests. The natural water matrices were obtained from the Snake River (Clarkston, WA) and a local well (Pullman, WA). The results are presented in Table S1 along with non-spiked blank control data. Recoveries for the spiked atrazine samples were between 97.0% and 109% for the river water matrix, and between 90.8% and 101% for the well water matrix. Recoveries for the spiked acetochlor samples were between 92.4% and 112% for the river water matrix and between 102% and 117% for the well water matrix. These recoveries validate the reliability of the NEMEIS assay procedure for the herbicides of interest here and offer support for extending the procedure for fieldable detection of a host of small molecules.

4. Conclusions

In this work, we have successfully developed a novel multiplex immunosensor for simultaneous and rapid quantitative detection of herbicides, with the capability of detecting atrazine and acetochlor with LODs of 0.24 ppb and 3.2 ppb, respectively. The reliability of the biosensor process was evaluated by accessing the efficacy of detection in spiked samples, where data show recoveries in the 90.8–117% range. This excellent performance in terms of LOD and recoveries is attributed to the following aspects: i) Pd@Pt NPs have superior peroxidase-like activity and can be synthesized and used as the signal transducer; ii) the use of bifurcated paper-based LFIA allows rapid and multiplex detection of two targets without apparent interferences due to the presence of different herbicide analytes; iii) quantitative electrochemical analysis can be integrated with LFIA technique using a 3D-printed housing that allows a simple cut-out step to transfer LFIA test regions to a liquid filled chamber directly above the electrodes imbedded in the housing. These features provide advantages of low cost, good portability, and ease-of-operation. Though the proposed device only contains two channels for simultaneously detection of just two herbicides, the multiplexing may be extended easily to include more channels with the aid of prototyping by additive manufacturing. The portability may be further improved by employing a portable electrochemical analyzer or smartphone-based electrochemical module. We expect the NEMEIS, as supported by the results, to provide a promising 3D-printed housing for bifurcated test strips and electrodes that will allow a rapid, precise, economical, and portable detection device for herbicides.

CRediT authorship contribution statement

Xiaofan Ruan: Conceptualization, Methodology, Writing – original draft, preparation. **Yijia Wang:** Conceptualization. **Eunice Y. Kwon:** Methodology, Writing – original draft, preparation. **Limin Wang:** Methodology. **Nan Cheng:** Methodology, Investigation. **Xiangheng Niu:** Methodology, Investigation. **Shichao Ding:** Methodology. **Bernard J. Van Wie:** Supervision, Writing – review & editing. **Yuehe Lin:** Supervision. **Dan Du:** Supervision, Writing – review & editing.

Declaration of competing interest

The authors declare that they have no known competing financial interests or personal relationships that could have appeared to influence the work reported in this paper.

Acknowledgements

This work was supported by the United States Department of Agriculture (USDA) National Institute of Food and Agriculture, AFRI project [grant number 2018-67021-27970].

Appendix A. Supplementary data

Supplementary data to this article can be found online at https://doi.org/10.1016/j.bios.2021.113238.

References

Ambrosi, A., Pumera, M., 2016. 3D-printing technologies for electrochemical applications. Chem. Soc. Rev. 45, 2740–2755.

An, B.W., Kim, K., Lee, H., Kim, S.-Y., Shim, Y., Lee, D.-Y., Song, J.Y., Park, J.-U., 2015. High-Resolution printing of 3D structures using an electrohydrodynamic inkjet with multiple functional inks. Adv. Mater. 27, 4322–4328.

Arregui, M.C., Sánchez, D., Althaus, R., Scotta, R.R., Bertolaccini, I., 2010. Assessing the risk of pesticide environmental impact in several Argentinian cropping systems with a fuzzy expert indicator. Pest Manag. Sci. 66, 736–740.

Cesarino, I., Moraes, F.C., Lanza, M.R.V., Machado, S.A.S., 2012. Electrochemical detection of carbamate pesticides in fruit and vegetables with a biosensor based on acetylcholinesterase immobilised on a composite of polyaniline–carbon nanotubes. Food Chem. 135, 873–879.

Cevenini, L., Calabretta, M.M., Tarantino, G., Michelini, E., Roda, A., 2016. Smartphone-interfaced 3D printed toxicity biosensor integrating bioluminescent "sentinel cells. Sensor. Actuator. B Chem. 225, 249–257.

Cheng, N., Song, Y., Zeinhom, M.M.A., Chang, Y.-C., Sheng, L., Li, H., Du, D., Li, L., Zhu, M.-J., Luo, Y., Xu, W., Lin, Y., 2017. Nanozyme-mediated dual immunoassay integrated with smartphone for use in simultaneous detection of pathogens. ACS Appl. Mater. Interfaces 9, 40671–40680.

Choi, H., Son, S.E., Hur, W., Tran, V.K., Lee, H.B.B., Park, Y., Han, D.K., Seong, G.H., 2020. Electrochemical immunoassay for determination of glycated albumin using nanozymes. Sci. Rep. 10, 1–12.

Choi, J., Gani, A.W., Bechstein, D.J.B., Lee, J.R., Utz, P.J., Wang, S.X., 2016. Portable, one-step, and rapid GMR biosensor platform with smartphone interface. Biosens. Bioelectron. 85, 1–7.

Deryabina, M.A., Yakovleva, Y.N., Popova, V.A., Eremin, S.A., 2005. Determination of the herbicide acetochlor by fluorescence polarization immunoassay. J. Anal. Chem. 60, 80–85.

Dou, Y., Jiang, Z., Deng, W., Su, J., Chen, S., Song, H., Aldalbahi, A., Zuo, X., Song, S., Shi, J., Fan, C., 2016. Portable detection of clenbuterol using a smartphone-based electrochemical biosensor with electric field-driven acceleration. J. Electroanal. Chem. 781, 339–344.

Du, D., Wang, L., Shao, Y., Wang, J., Engelhard, M.H., Lin, Y., 2011. Functionalized graphene oxide as a nanocarrier in a multienzyme labeling amplification strategy for ultrasensitive electrochemical immunoassay of phosphorylated p53 (S392). Anal. Chem. 83, 746–752.

Du, D., Zou, Z., Shin, Y., Wang, J., Wu, H., Engelhard, M.H., Liu, J., Aksay, I.A., Lin, Y., 2010. Sensitive immunosensor for cancer biomarker based on dual signal amplification strategy of graphene sheets and multienzyme functionalized carbon nanospheres. Anal. Chem. 82, 2989–2995.

Du, Y., Dong, S., 2017. Nucleic acid biosensors: recent advances and perspectives. Anal. Chem. 89, 189–215.

Fu, S., Zhu, C., Shi, Q., Xia, H., Du, D., Lin, Y., 2016. Highly branched PtCu bimetallic alloy nanodendrites with superior electrocatalytic activities for oxygen reduction reactions. Nanoscale 8, 5076–5081.

Gross, B., Lockwood, S.Y., Spence, D.M., 2017. Recent advances in analytical chemistry by 3D printing. Anal. Chem. 89, 57–70.

Ho, E.H.Z., Ambrosi, A., Pumera, M., 2018. Additive manufacturing of electrochemical interfaces: simultaneous detection of biomarkers. Appl. Mater. Today 12, 43–50.

Hossain, M.F., Park, J.Y., 2014. Amperometric glucose biosensor based on Pt-Pd nanoparticles supported by reduced graphene oxide and integrated with glucose oxidase. Electroanalysis 26, 940–951.

Huang, Y., Ren, J., Qu, X., 2019. Nanozymes: classification, catalytic mechanisms, activity regulation, and applications. Chem. Rev. 119, 4357–4412.

Hvězdová, M., Kosubová, P., Košíková, M., Scherr, K.E., Šimek, Z., Brodský, L., Šudoma, M., Škulcová, L., Sáňka, M., Svobodová, M., Krkošková, L., Vašíčková, J., Neuwirthová, N., Bielská, L., Hofman, J., 2018. Currently and recently used pesticides in Central European arable soils. Sci. Total Environ. 613–614, 361–370.

Jayanthi, V.S.P., Das, A.B., Saxena, U., 2017. Recent advances in biosensor development for the detection of cancer biomarkers. Biosens. Bioelectron. 91, 15–23.

Ji, D., Liu, L., Li, S., Chen, C., Lu, Y., Wu, J., Liu, Q., 2017. Smartphone-based cyclic voltammetry system with graphene modified screen printed electrodes for glucose detection. Biosens. Bioelectron. 98, 449–456.

Jiang, T., Song, Y., Du, D., Liu, X., Lin, Y., 2016. Detection of p53 protein based on mesoporous Pt-Pd nanoparticles with enhanced peroxidase-like catalysis. ACS Sens. 1, 717–724.

Kaur, J., Singh, K.V., Boro, R., Thampi, K.R., Raje, M., Varshney, G.C., Suri, C.R., 2007. Immunochromatographic dipstick assay format using gold nanoparticles labeled protein-hapten conjugate for the detection of atrazine. Environ. Sci. Technol. 41, 5028–5036.

Kumar, N., Hu, Y., Singh, S., Mizaikoff, B., 2018. Emerging biosensor platforms for the assessment of water-borne pathogens. Analyst 143, 359–373.

Kurbanoglu, S., Ozkan, S.A., Merkoçi, A., 2017. Nanomaterials-based enzyme electrochemical biosensors operating through inhibition for biosensing applications. Biosens. Bioelectron. 89, 886–898.

Kwon, E.Y., Ruan, X., Wang, L., Lin, Y., Du, D., Van Wie, B.J., 2020. Mesoporous Pd@Pt nanoparticle-linked immunosorbent assay for detection of atrazine. Anal. Chim. Acta 1116, 36–44.

Liu, K., Dong, H., Deng, Y., 2016. Recent advances on rapid detection of pesticides based on enzyme biosensor of nanomaterials. J. Nanosci. Nanotechnol. 16, 6648–6656.

Liu, R., Guan, G., Wang, S., Zhang, Z., 2011. Core-shell nanostructured molecular imprinting fluorescent chemosensor for selective detection of atrazine herbicide. Analyst 136, 184–190.

Liu, Z., Fu, Z., Jin, Y., 2017. Immunotoxic effects of atrazine and its main metabolites at environmental relevant concentrations on larval zebrafish (Danio rerio). Chemosphere 166, 212–220.

Maduraiveeran, G., Sasidharan, M., Ganesan, V., 2018. Electrochemical sensor and biosensor platforms based on advanced nanomaterials for biological and biomedical applications. Biosens. Bioelectron. 103, 113–129.

Mahato, K., Srivastava, A., Chandra, P., 2017. Paper based diagnostics for personalized health care: emerging technologies and commercial aspects. Biosens. Bioelectron. 96, 246–259.

Mao, M., He, J., Li, X., Zhang, B., Lei, Q., Liu, Y., Li, D., 2017. The emerging frontiers and applications of high-resolution 3D printing. Micromachines 8, 1–20.

Mehrotra, P., 2016. Biosensors and their applications – a review. J. Oral Biol. Craniofacial Res. 6, 153–159.

Mettakoonpitak, J., Boehle, K., Nantaphol, S., Teengam, P., Adkins, J.A., Srisa-Art, M., Henry, C.S., 2016. Electrochemistry on paper-based analytical devices: a review. Electroanalysis 28, 1420–1436.

Mudanyali, O., Dimitrov, S., Sikora, U., Padmanabhan, S., Navruz, I., Ozcan, A., 2012. Integrated rapid-diagnostic-test reader platform on a cellphone. Lab Chip 12, 2678–2686.

Niu, X., Li, X., Lyu, Z., Pan, J., Ding, S., Ruan, X., Zhu, W., Du, D., Lin, Y., 2020. Metal-organic framework based nanozymes: promising materials for biochemical analysis. Chem. Commun. 56, 11338–11353.

Pai, N.P., Tulsky, J.P., Cohan, D., Colford, J.M., Reingold, A.L., 2007. Rapid point-of-care HIV testing in pregnant women: a systematic review and meta-analysis. Trop. Med. Int. Health 12, 162–173.

Rim, Y.S., Bae, S.H., Chen, H., De Marco, N., Yang, Y., 2016. Recent progress in materials and devices toward printable and flexible sensors. Adv. Mater. 28, 4415–4440.

Roda, A., Guardigli, M., Calabria, D., Calabretta, M.M., Cevenini, L., Michelini, E., 2014. A 3D-printed device for a smartphone-based chemiluminescence biosensor for lactate in oral fluid and sweat. Analyst 139, 6494–6501.

Ruan, X., Wang, Y., Cheng, N., Niu, X., Chang, Y., Li, L., Du, D., Lin, Y., 2020. Emerging applications of additive manufacturing in biosensors and bioanalytical devices. Adv. Mater. Technol. 5, 2000171.

Sahin, B., Kaya, T., 2019. Electrochemical amperometric biosensor applications of nanostructured metal oxides: a review. Mater. Res. Express 6, 042003.

Sajid, M., Kawde, A.-N., Daud, M., 2015. Designs, formats and applications of lateral flow assay: a literature review. J. Saudi Chem. Soc. 19, 689–705.

Sharafeldin, M., Jones, A., Rusling, J.F., 2018. 3D-printed biosensor arrays for medical diagnostics. Micromachines 9, 1–22.

Shu, J., Tang, D., 2017. Current advances in quantum-dots-based photoelectrochemical immunoassays. Chem. Asian J. 12, 2780–2789.

Skládal, P., 1997. Advances in electrochemical immunosensors. Electroanalysis 9, 737–745.

Sousa, J.C.G., Ribeiro, A.R., Barbosa, M.O., Pereira, M.F.R., Silva, A.M.T., 2018. A review on environmental monitoring of water organic pollutants identified by EU guidelines. J. Hazard Mater. 344, 146–162.

Taleat, Z., Khoshroo, A., Mazloum-Ardakani, M., 2014. Screen-printed electrodes for biosensing: a review (2008–2013). Microchim. Acta 181, 865–891.

Tan, W., Hu, X., Yang, M., Barrow, C.J., Yang, W., Wang, H., 2014. Analysis of residues of prometryne and acetochlor in soil-water system by solid-phase extraction and gas chromatography/mass spectrometry. Desalin. Water Treat. 52, 1177–1182.

Tang, Z., Du, X., Louie, R.F., Kost, G.J., 2000. Effects of drugs on glucose measurements with handheld glucose meters and a portable glucose analyzer. Am. J. Clin. Pathol. 113, 75–86.

Wang, Q., Wei, H., Zhang, Z., Wang, E., Dong, S., 2018. Nanozyme: an emerging alternative to natural enzyme for biosensing and immunoassay. Trends Anal. Chem. 105, 218–224.

Wang, Y., Zeinhom, M.M.A., Yang, M., Sun, R., Wang, S., Smith, J.N., Timchalk, C., Li, L., Lin, Y., Du, D., 2017. A 3D-printed, portable, optical-sensing platform for smartphones capable of detecting the herbicide 2,4-dichlorophenoxyacetic acid. Anal. Chem. 89, 9339–9346.

Xie, J., Zhao, L., Liu, K., Liu, W., 2019. Enantiomeric environmental behavior, oxidative stress and toxin release of harmful cyanobacteria Microcystis aeruginosa in response to napropamide and acetochlor. Environ. Pollut. 246, 728–733.

Yu, Q., Zhang, P., He, Y., Xu, Z., He, X., Hu, Y., Zhang, H., He, L., 2019. Dissipation dynamics and residue of four herbicides in paddy fields using HPLC-MS/MS and GC-MS. Int. J. Environ. Res. Publ. Health 16, 236–250.

Yuan, C.X., Fan, Y.R., Tao-Zhang, Guo, H.X., Zhang, J.X., Wang, Y.L., Shan, D.L., Lu, X. Q., 2014. A new electrochemical sensor of nitro aromatic compound based on three-dimensional porous Pt-Pd nanoparticles supported by graphene-multiwalled carbon nanotube composite. Biosens. Bioelectron. 58, 85–91.

Yuan, G., Zhang, R., Chen, X., Wang, B., Guo, R., 2018. A simple and economical method of gas chromatography-mass spectrometry to determine the presence of 6 pesticides in human plasma and its clinical application in patients with acute poisoning. Biosci. Trends 12, 201–207.

Zamaleeva, A.I., Sharipova, I.R., Shamagsumova, R.V., Ivanov, A.N., Evtugyn, G.A., Ishmuchametova, D.G., Fakhrullin, R.F., 2011. A whole-cell amperometric herbicide biosensor based on magnetically functionalised microalgae and screen-printed electrodes. Anal. Methods 3, 509–513.

Zhang, B., He, J., Li, X., Xu, F., Li, D., 2016. Micro/nanoscale electrohydrodynamic printing: from 2D to 3D. Nanoscale 8, 15376–15388.

Zhang, D., Liu, Q., 2016. Biosensors and bioelectronics on smartphone for portable biochemical detection. Biosens. Bioelectron. 75, 273–284.

Zhao, Q., Li, H., Xu, Y., Zhang, F., Zhao, J., Wang, L., Hou, J., Ding, H., Li, Y., Jin, H., Ding, L., 2015. Determination triazine pesticides in cereal samples based on single-hole hollow molecularly imprinted microspheres. J. Chromatogr. A 1376, 26–34.

Zhao, Y., Yang, M., Fu, Q., Ouyang, H., Wen, W., Song, Y., Zhu, C., Lin, Y., Du, D., 2018. A nanozyme- and ambient light-based smartphone platform for simultaneous detection of dual biomarkers from exposure to organophosphorus pesticides. Anal. Chem. 90, 7391–7398.

Zhou, Y., Xiao, J., Ma, X., Wang, Q., Zhang, Y., 2018. An effective established biosensor of bifunctional probes-labeled AuNPs combined with LAMP for detection of fish pathogen Streptococcus iniae. Appl. Microbiol. Biotechnol. 102, 5299–5308.

Zhu, C., Yang, G., Li, H., Du, D., Lin, Y., 2015. Electrochemical sensors and biosensors based on nanomaterials and nanostructures. Anal. Chem. 87, 230–249.

Zou, Z., Du, D., Wang, J., Smith, J.N., Timchalk, C., Li, Y., Lin, Y., 2010. Quantum dot-based immunochromatographic fluorescent biosensor for biomonitoring trichloropyridinol, a biomarker of exposure to chlorpyrifos. Anal. Chem. 82, 5125–5133.